



Surface temperature patterns in complex terrain: Daily variations and long-term change in the central Sierra Nevada, California

Jessica D. Lundquist^{1,2} and Daniel R. Cayan^{3,4}

Received 25 May 2006; revised 7 February 2007; accepted 22 February 2007; published 14 June 2007.

[1] A realistic description of how temperatures vary with elevation is crucial for ecosystem studies and for models of basin-scale snowmelt and spring streamflow. This paper explores surface temperature variability using temperature data from an array of 37 sensors, called the Yosemite network, which traverses both slopes of the Sierra Nevada in the vicinity of Yosemite National Park, California. These data indicate that a simple lapse rate is often a poor description of the spatial temperature structure. Rather, the spatial pattern of temperature over the Yosemite network varies considerably with synoptic conditions. Empirical orthogonal functions (EOFs) were used to identify the dominant spatial temperature patterns and how they vary in time. Temporal variations of these surface temperature patterns were correlated with large-scale weather conditions, as described by National Centers for Environmental Prediction-National Center for Atmospheric Research Reanalysis data. Regression equations were used to downscale larger-scale weather parameters, such as Reanalysis winds and pressure, to the surface temperature structure over the Yosemite network. These relationships demonstrate that strong westerly winds are associated with relatively warmer temperatures on the east slope and cooler temperatures on the west slope of the Sierra, and weaker westerly winds are associated with the opposite pattern. Reanalysis data from 1948 to 2005 indicate weakening westerlies over this time period, a trend leading to relatively cooler temperatures on the east slope over decadal timescales. This trend also appears in long-term observations and demonstrates the need to consider topographic effects when examining long-term changes in mountain regions.

Citation: Lundquist, J. D., and D. R. Cayan (2007), Surface temperature patterns in complex terrain: Daily variations and long-term change in the central Sierra Nevada, California, *J. Geophys. Res.*, 112, D11124, doi:10.1029/2006JD007561.

1. Introduction

[2] A realistic description of how temperatures vary over mountain terrain is crucial for models of basin-scale snowmelt and spring streamflow [Archer, 2004; Singh, 1991], especially in the western United States, where snowmelt supplies over 50% of water resources. Accurate descriptions of temperature structure are also necessary to understand ecological distributions across space and time [Chen *et al.*, 1999]. However, measurements at high elevations are scarce, and besides varying with elevation, observed surface temperatures vary diurnally, synoptically, and seasonally according to other topographic characteristics [Rolland, 2003].

[3] Mountain temperature variability is complicated because it encompasses such a broad range of temporal and spatial scales. Spatially intensive studies of topographically controlled temperature variations, such as nocturnal

drainage [Neff and King, 1989], generally span only a few days to weeks in time, while multidecadal studies of climatic change generally examine only a small number of high elevation stations per region [Diaz and Bradley, 1997; Pepin, 2000]. For most forecasts of mountain temperatures and input to snowmelt models, temperature is determined at each elevation based on either a standard atmospheric lapse rate, $-6.5^{\circ}\text{C km}^{-1}$ [Martinez and Rango, 1986], or a spatially varied but climatically fixed lapse rate determined by month or by year from historical data at nearby stations [PRISM, Daly *et al.*, 2002]. These approaches cannot account for day-to-day variations in the vertical or spatial temperature structure. Some models use a linear lapse rate derived from available nearby surface measurements [Daly *et al.*, 2000], but this approach is limited by the number of surface measurements available and cannot account for nonlinear variations. Work is needed to bridge the gap between spatially dense short-term observations and a sparse network of longer-term observations. Particularly, we need to describe how fine-spatial-scale variations evolve in time: when are spatial variations most pronounced, and what errors are incurred by neglecting these variations.

[4] The gap between scales is particularly evident in studies of long-term temperature trends, which demonstrate

¹Cooperative Institute for Research in Environmental Sciences—NOAA Earth Systems Laboratory, Boulder, Colorado, USA.

²Now at University of Washington, Seattle, Washington, USA.

³Scripps Institution of Oceanography, La Jolla, California, USA.

⁴U. S. Geological Survey, La Jolla, California, USA.

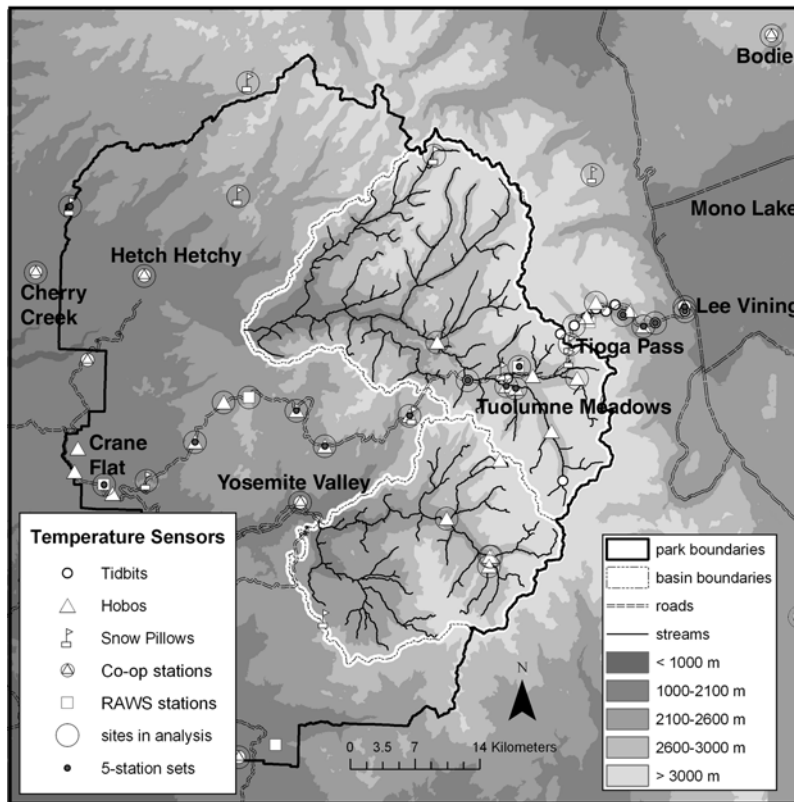


Figure 1. Map of Yosemite network sensors. Yosemite National Park is located in the central Sierra Nevada of California. Elevation zones correspond to different vegetation zones: lower montane (~ 1000 – 2100 m, Ponderosa Pine), upper montane (~ 2100 – 2600 m, Red Fir, Jeffrey Pine, and Western Juniper), and subalpine (~ 2600 – 3000 m, Lodgepole Pine, Whitebark Pine, and Mountain Hemlock) forests on the west slope, and between upper montane (~ 3000 – 2600 m), lower montane (~ 2600 – 2100 m), and piñon pine, juniper, and aspen (< 2100 m) forests on the east slope.

threats to snow and regional water supplies [Dettinger *et al.*, 2004; Hamlet *et al.*, 2005; Knowles *et al.*, 2006]. Studies of mountain climate have reached strikingly different conclusions about whether the high mountains are warming faster or slower than the lowlands, ranging from the western European Alps, where higher elevations are warming significantly faster than lower elevations [Beniston *et al.*, 1997; Diaz and Bradley, 1997] to the Rocky Mountains west of Denver, Colorado, where high elevations have been cooling over recent decades [Pepin, 2000; Pepin and Losleben, 2002]. Differences have been noted both between mountain ranges [Diaz and Bradley, 1997] and between sites within a given mountain range [Pepin *et al.*, 2005]. Changes in large-scale circulation patterns may be at least partially responsible for this wide range of results, since changes in cloudiness, snow cover, and winds affect sites with varying topographic orientations differently [Pepin and Norris, 2005; Richner and Phillips, 1984]. In addition, many of the sites used in the above mentioned climate studies were located in valley bottoms, where local inversions and cold air drainage may make a long-term measurement site unrepresentative of temperatures across most of the surrounding topography [Rolland, 2003].

[5] The objectives of this paper are to (1) demonstrate that mountain temperatures vary in systematic spatial pat-

terns that cannot be adequately represented by linear lapse rates; (2) illustrate how these spatially complex temperature patterns evolve through time and how they can be estimated at times when high-density temperature data are not available (for snowmelt modeling); and (3) explore connections between spatially dense but short-term measurements and spatially sparse but long-term measurements to provide a context for interpreting long-term changes (for climate modeling). To achieve these goals, we used a prototypical array of over 40 temperature sensors in the region of Yosemite National Park, California (Figure 1), to demonstrate how surface temperatures vary over synoptic to seasonal timescales in complex terrain. These sensors included both standard meteorological stations and small, low-cost, self-recording temperature loggers (section 2). First, we examined the limitations of linear fits to the data (section 3.1). Second, we used empirical orthogonal functions (EOFs) to identify key patterns of spatial variability (section 3.2). Third, we related these spatial modes to larger scale atmospheric conditions, using National Centers for Environmental Prediction-National Center for Atmospheric Research (NCEP-NCAR) Reanalysis data and regression analysis, to predict how surface temperature distributions would change in different synoptic weather regimes (section 3.3). Finally, we looked at long term trends in the

Table 1. Sensor Types and Characteristics

Description	Onset Hobos	Onset Stowaway Tidbits	California Snow Survey Stations	Remote Automated Weather Stations (RAWS)	Cooperative Observer (Co-op) Stations
	Fist-sized, self-recording temperature and relative humidity	Quarter-sized, self-recording temperature	Standard temperature sensors	Standard temperature sensors	Ventilated, sheltered thermometer
Site Characteristics	In small radiation shields on north-facing side of tree on edge of forest	In small radiation shields on north-facing side of tree on edge of forest	In beehive radiation shields, on pole in the middle of a small clearing or meadow	In beehive radiation shields, on pole in the middle of a small clearing or meadow	Generally in a Stevenson Screen in a level, open clearing
Height Above Ground	4 to 8 m	4 to 8 m	10 m	6 m	2–3 m
Sampling Frequency	30 min	30 min	60 min	15 min	Max/min written down once daily
Agency in Charge	Scripps Institution of Oceanography	Scripps Institution of Oceanography	California Department of Water Resources (CA DWR)	National Interagency Fire Center	National Weather Service (NWS)
Number of Sensors in Network (Number Used in Analysis)	23 (15)	11 (5)	11 (7)	5 (3)	9 (7)
Data Location	Available from authors on request	Available from authors on request	CA DWR http://cdec.water.ca.org	Western Regional Climate Center http://www.yosemite.dri.edu/index.htm	National Climatic Data Center http://lwf.ncdc.noaa.gov/oa/climate/climateata.html
Time Frame for Measurements	Summer 2001 to present, # sensors changed with time	Summer 2001 to present, # sensors changed with time	Since mid-1980s at most stations	Since early 1990s at most stations	Since mid-1950s at most stations

relevant synoptic patterns to examine how climate signals may have been expressed differently in various mountain locations over the past 50 years (section 3.4). Results, summary, and conclusions are presented in section 4.

2. Data and Methods

2.1. Surface Temperatures: Yosemite Temperature Network

[6] The Tioga Road (California Route 120) is the highest road passing over the Sierra Nevada, and traverses the west slope of the Sierra Nevada through Yosemite National Park and the east slope through Lee Vining Canyon and down into the Owens Valley. Given the large range of elevations and the availability of several existing weather stations at key locations along the road, the Tioga Road was selected as a transect to monitor hydroclimatic variability across the Sierra [Lundquist *et al.*, 2003]. Sensors across this transect included small, inexpensive, self-recording temperature sensors, which sampled at hourly intervals and whose data were manually retrieved and downloaded each year, and more traditional temperature sensors, which provided telemetered, real-time hourly or daily maximum and minimum temperature data (Figure 1). Table 1 details the different data sources used in this study, which are collectively called the Yosemite network. Throughout the analyses, sensor types were labeled to determine if there were discernable effects from different sensors and their individual site-specific conditions. These are discussed in section 4. Throughout the paper, the term “surface temperatures” refers to these (2 to 10 m high) sensors and not to the actual ground surface.

[7] Daily mean, maximum, and minimum temperatures (T_{surf}) were calculated for each automatically recording sensor for the period of 0:00 to 23:00 LST, and daily means were calculated as the average of the reported maximum and minimum temperatures at each coop station. All data were manually checked, and extreme outliers and inconsistencies were flagged and omitted from subsequent analyses. The time period was limited to that in which more than 35 stations were reporting, resulting in an analysis period from 17 July 2002 to 30 June 2004. To eliminate poorly sampled stations, only stations having more than 630 days of valid data during that period were included in the EOF calculations. This limited the analysis to 37 of the 62 potential stations in the network (marked, Figure 1). Each station’s temporal mean temperature ($\langle T_{surf} \rangle$) over the July 2002 through June 2004 study period was calculated (Figure 2) and then removed from each record prior to EOF analysis ($T'_{surf} = T_{surf} - \langle T_{surf} \rangle$).

2.2. Free-Air Temperatures: Oakland Radiosonde and Reanalysis Data

[8] Upper air measurements of temperature, humidity, wind speed and direction were obtained from the NOAA National Weather Service Radiosonde Network site at Oakland, California, which is upwind of Yosemite and represents free-air conditions before the air encounters the topography of the Sierra. Radiosondes measure these parameters at 0 and 12 UTC (0400 and 1600, PST) each day.

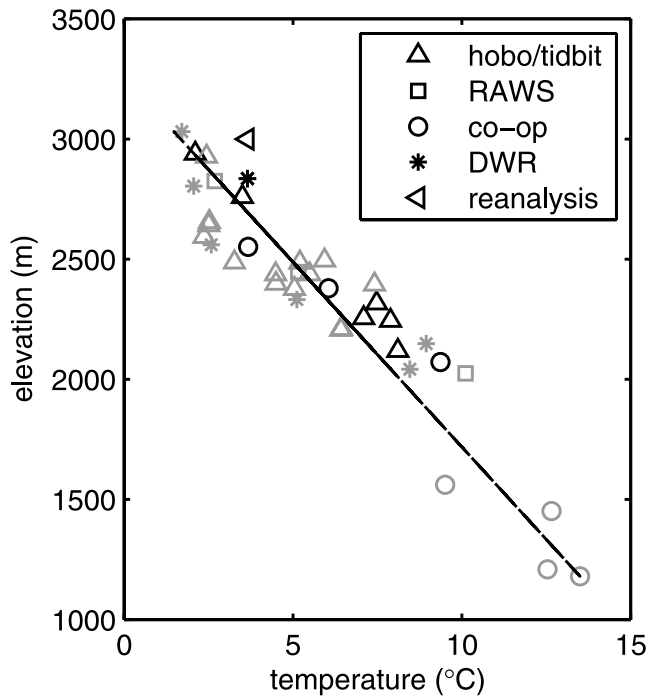


Figure 2. Average temperature at each measured location between 17 July 2002 and 30 June 2004, compared with the standard lapse rate of -6.5°C per km. Gray symbols represent west slope sites; black symbols represent east slope sites. Different station or sensor types are shown in the legend.

[9] Gridded upper-air analyses (temperature, height, winds, and humidities) for the Northern Hemisphere for 1948 to 2005 were obtained from NCEP-NCAR Reanalysis 1 data [Kalnay *et al.*, 1996] (hereafter designated as Reanalysis). Time series for 700 hPa parameters of temperature (T_{700}), geopotential height, relative humidity, specific humidity, and zonal, meridional, and vertical winds were obtained for the 2.5° grid cell over the Yosemite study area (37.5°N , 120°W). The 700-hPa level is at an altitude of approximately 3000 m, which is about the elevation of the highest sensors in the Yosemite Network. Thus it is representative of free-air temperature (combining real-time observations and models) at the level it intersects the mountaintops. The July 2002 through June 2004 mean temperature ($\langle T_{700} \rangle$) was removed prior to further analyses ($T'_{700} = T_{700} - \langle T_{700} \rangle$).

2.3. EOFs and Associated Analyses

[10] EOFs can be constructed using singular value decomposition (SVD, Anderson *et al.* [1999]) to decompose a data set into its principal spatial patterns of variation and their evolution through time [Preisendorfer, 1988]. The EOFs are linear and orthogonal, such that a sum of each spatial component multiplied by its corresponding temporal variation recreates the original temperature data set, and are normalized, such that the variances of all components sum to one. Because the Yosemite network domain is smaller than synoptic weather systems, the predominant spatial pattern of the raw data is that all locations vary together (i.e., if one site is warmer, all are warmer), where each site

has a weight proportional to its mean temperature for the analysis period. The corresponding temporal evolution (here referred to as the principal component, PC) of this pattern represents spatially averaged temperature fluctuations over the region.

[11] In this study, we are interested in how sites within the Yosemite Network differ from regional estimates of temperature (represented here by the Reanalysis data) and from each other over time. Thus we set up the analysis to focus on spatial variations from the regional mean. With this in mind, the 700 hPa temperature residuals (T'_{700}), representing the regional average temperature fluctuations, were considered a “known” baseline and were removed from the surface temperature residuals (T'_{surf}). Thus the resulting surface temperature anomalies can be considered as departures from 700 hPa free air temperature anomalies ($T'_{\text{var}} = T'_{\text{surf}} - T'_{700}$).

[12] We calculated EOFs of these temperature variations (T'_{var}) based on the method of Beckers and Rixen [2003]. This method allows for short periods of missing data by using a series of iteratively calculated EOFs, employing the singular value decomposition algorithm [Anderson *et al.*, 1999] from Matlab, to fill data gaps. We calculated the optimal number of EOFs by arbitrarily removing 50 randomly chosen data points, calculating EOFs from the remaining data points, and then checking how well various subsets of EOFs (starting with just the first and then adding one EOF at a time) represented the values at the missing data points. In this data set, the first four EOFs each greatly reduced the error, and EOFs 5, 6, and 7 made only marginal improvements. Including more than seven EOFs increased the error in the estimation. Thus we confine the present analysis to EOFs 1–4.

[13] The dominant weather patterns associated with the occurrence of particular EOF patterns were determined by selecting the dates in the EOF’s temporal PC series with an amplitude greater than one standard deviation above the mean (high values) and the dates with an amplitude less than one standard deviation below the mean (low values). Weather patterns associated with high or low values were determined by averaging selected atmospheric variables on the selected dates, using the NOAA-CIRES Climate Diagnostics Center software (<http://www.cdc.noaa.gov>). Also, correlations between the PCs of each of the first four EOFs and selected 700-hPa parameters were calculated to identify the weather parameters associated with each of the small-scale temperature patterns.

[14] Relationships between surface temperature patterns and larger-scale weather patterns were determined using regression analyses, with Reanalysis variables from the grid cell at the latitude, longitude, and elevation closest to the study area (37.5°N , 120°W , 700 hPa) serving as predictors to estimate the PCs of each EOF. Each of these input variables were scaled to have a mean of 0 and a standard deviation of 1, so that the size of each regression coefficient represented the importance of each term’s contribution to the predictive equation. We used stepwise linear regression [Draper and Smith, 1981] to determine the coefficients of statistically significant terms while removing insignificant variables from the predictive equation (p value must be less than 0.0001 to add a term and p value greater than 0.0002 warrants removing a term).

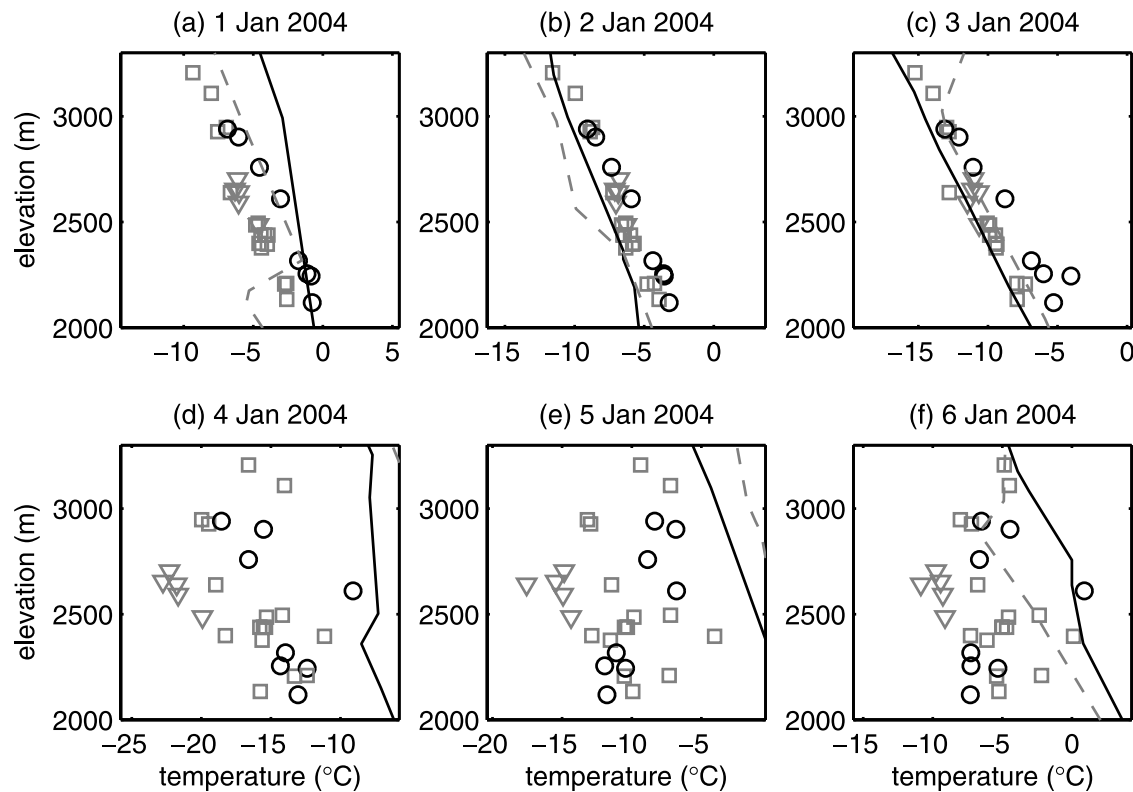


Figure 3. Temperature versus elevation for six days in January 2004. Gray dashed line is morning (0400 PST) sounding at Oakland; black solid line is afternoon (1600 PST) sounding at Oakland. Black circles are average daily temperatures at east slope stations; grey symbols are west slope stations, where triangles represent stations in the Tuolumne Meadows region, and squares represent stations along the Tioga Road. Note: In Figure 3d, the dashed line is off the scale because the morning sounding was even warmer than the afternoon sounding.

[15] The PCs estimated by the regression equations were then combined with the spatial EOFs from the original 2002–2004 data set to determine temperatures over the complex terrain of the Yosemite network. “Predicted” temperature fluctuations were calculated over 2002–2005 with various levels of spatial modifications: (1) base prediction = 2-year mean temperature at each station modified by free-air temperature deviations; (2) base plus fluctuations at each station from the estimated PC of EOF 1; and (3) base plus fluctuations from the estimated PCs of EOFs 1 and 2. For the 2002–2004 analysis period only, the latter two predictions were also made using the calculated PCs, to determine the best skill that could be obtained with only the first one or two EOFs if their PCs were perfectly known.

[16] To quantify how the modeled PCs reduced the root mean squared error (RMSE) of the estimated temperatures in different geographic locations, five representative stations were selected for each of the east slope, west slope, and Tuolumne Meadows region of Yosemite (Figure 1). These stations were selected because of their reliable data records throughout 2002–2005 and because of their strong response weights in the EOF patterns. RMSEs of predicted versus measured temperatures for the representative stations from each region were calculated for both the 2-year analysis period and the 2004–2005 validation period, where the 2004–2005 time period demonstrated the performance that

could be expected when applying the regression models to periods not included in their calibration.

3. Results and Discussion

3.1. Is a Lapse Rate Representative? Case Study: January 2004

[17] As a description of average conditions, i.e., 2-year mean temperatures at the 37 stations with substantial data (section 2.1), a linear lapse rate is a reasonable model of the temperature structure in the Yosemite network (Figure 2). The RMS errors between the data and lines based on both a linear fit to the data (slope of $-6.8^{\circ}\text{C km}^{-1}$) and the standard lapse rate are 1.1°C . However, the daily data (Figure 3) reveal that temperatures only sometimes decrease linearly with elevation. On 1 to 3 January 2004, the weather in the Yosemite region was dominated by a low-pressure system with strong westerly winds. Temperatures decreased linearly with elevation and matched closely with free-air temperatures observed by the Oakland sounding (Figures 3a–3c). However, by 4 January 2004, the low-pressure system migrated eastward, and high pressure developed over the study area. Wind speeds greatly decreased. Clear skies and frigid temperatures (daily means ranging from -8° to -24°C) resulted in cold-air drainage to the meadows and valleys, and mean daily temperatures at many Yosemite sites

Table 2. Root Mean Squared Error (RMSE) in Temperature ($^{\circ}\text{C}$) for Yosemite Regional Sensors Calculated by Various Linear Lapse Rates Averaged From 17 July 2002 to 30 June 2004

	All stations	West	East	Meadow
Base Temp, $6.5^{\circ}\text{C km}^{-1}$	2.17	2.00	2.59	2.21
Lapse fit to Oakland Sounding (Surface to 500 hPa)	3.77	3.19	4.44	3.54
Lapse Fit to All Stations	1.70	1.81	2.15	1.69
Lapse Fit to Cooperative Stations	2.24	2.27	1.95	2.34
Lapse Fit to CA DWR Stations	2.20	1.57	2.92	1.83

were over 15°C cooler than those measured at equivalent elevations at Oakland (Figure 3d). The flattest locations, particularly those in the bottom of broad, U-shaped valleys, such as the Tuolumne Meadows area stations in the Yosemite network, became the coldest, so that temperatures increased with elevation above these areas. Temperatures continued to be uncorrelated with elevation over the next 2 days (Figures 3e–3f), suggesting that topographic characteristics other than elevation were exerting strong controls on temperatures across the landscape. This example illustrates the need to determine how patterns vary spatially, rather than focusing specifically on temperature changes with elevation.

[18] Over the entire July 2002–June 2004 data set, temperatures on any particular day exhibited substantial differences from both the standard lapse rate and a linear temperature approximation. Table 2 details the departures for temperatures calculated using linear lapse rates for the 37 stations with substantial data. Root-mean square errors (RMSEs), averaged over the 2-year period, were compared for lapse rates fitted to five different models: (1) the standard lapse rate of $-6.5^{\circ}\text{C km}^{-1}$ above the lowest elevation station (Hetch Hetchy Reservoir), (2) a linear fit to the Oakland sounding temperatures from the surface to 500 hPa, (3) a linear fit to all of the stations, (4) a linear fit to the cooperative observing stations, which have the longest records, and (5) a linear fit to the CA DWR stations, which provide data in real time. These calculations were based upon (1) all stations and (2) the sets of five representative stations from the east slope, west slope, and Tuolumne Meadows region. With the exception of the standard lapse rate, the linear fits were modified each day to best represent that day’s conditions. A standard lapse rate approximation yields average RMSEs of 2.17°C , approximately twice the size of the departures from the time averaged temperature profile in Figure 2. The fit to an arbitrary linear lapse rate using all of the surface tempera-

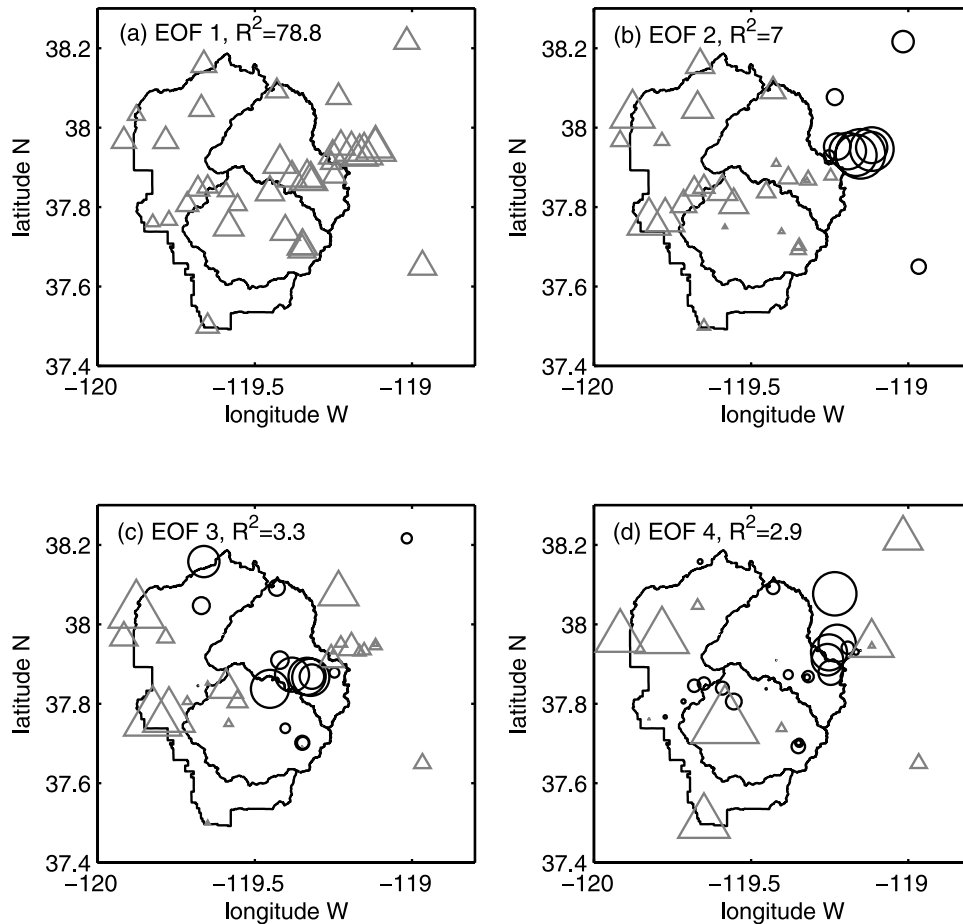


Figure 4. First four spatial EOFs for Yosemite temperatures. Grey triangles indicate positive; black circles indicate negative weights, and the size of the symbol indicates the magnitude of the weight for each station. Black outlines represent the park boundaries and the Tuolumne and Merced watersheds, thus defining the ridgelines (highest toward the northeast) within the area.

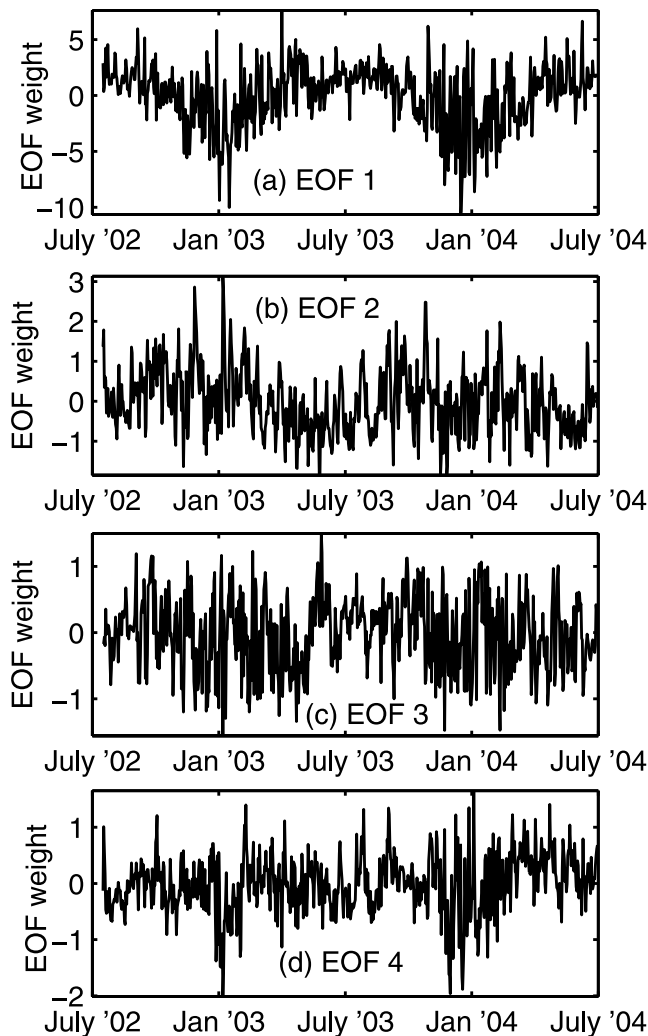


Figure 5. First four PCs, showing amplitudes of associated surface temperature EOFs in Figure 4 for each day, 17 July 2002 through 30 June 2004.

ture stations resulted in smaller errors ($RMSE = 1.70^{\circ}C$) than the standard lapse rate approximation, but the lapse rate varied markedly, from -2.3 to $-10.2^{\circ}C km^{-1}$. The fit to the Oakland sounding free-air lapse rate produced the highest errors ($RMSE = 3.77^{\circ}C$). As shown below, accounting for spatial variations beyond a linear change with elevation yields a better model for surface temperature structure than any of these lapse rate approximations.

3.2. EOFs and Their Correlations With Large-Scale Parameters

[19] The first few EOFs represent the primary modes of variability of the residual temperature patterns across the Yosemite landscape (Figure 4). The temporal PC series corresponding to each of these spatial patterns of temperature (Figure 5) are characterized by relatively large amplitude short-term synoptic variability and also some prominent seasonal variability. Approximately 92% of the surface temperature residuals' variance was explained by the first four EOFs, which were retained because they represent physically meaningful patterns of variability. The analysis was applied to seasonal subsets of the data

(DJF, MAM, JJA, SON), and to the entire 3-year data set from 2002 to 2005 (not shown), and yielded essentially the same four modes of variability. The EOF analysis was also applied to maximum temperatures, minimum temperatures, and daily temperature ranges (not shown), which resulted in similar patterns as the mean temperatures. Although EOFs 3 and 4 account for small fractions of the total variance, they are presented here to identify their relations to topographic features in the landscape and to larger-scale weather patterns.

3.2.1. EOF 1: Overall Surface Temperature Warmer or Cooler Than Free-Air Temperature

[20] The first mode (EOF 1, 78.8% of the variance) is representative of a pattern having roughly uniform temperature deviations, of the same sign (all positive or all negative) over all of the stations in the Yosemite network (Figure 4a). Sites on the east slope and sites in relatively flat terrain, such as in Tuolumne Meadows, have a larger magnitude, i.e., greater difference from free-air temperatures, than sites on the western Tioga Road. EOF 1 has a strong seasonal structure, with predominantly positive weights in summer and negative weights in winter (Figure 5a), representing the strong tendency for surface temperatures to be warmer than the free-air temperature in summer, and cooler than the free-air temperature in winter, as expected from seasonal changes in solar radiation.

[21] The PC time series for EOF 1 also contains substantial synoptic scale variability. In any season, the expression of the EOF 1 pattern is strongest on days with a strong temperature gradient across California. The composite analysis demonstrates that high positive values of PC 1 (surface warmer than the free air) correspond to developing low pressures and cool temperatures (i.e., cold-air advection), as a 700 hPa trough moves in from the northwest (Figure 6). The individual days making up the composite show 700 hPa troughs moving into the study area, but the shape of the troughs varies widely. Conversely, negative values of PC 1 (surface cooler than the free-air) correspond to a ridge with warm-air advection (not shown), similar to the findings of *Pepin and Norris* [2005]. These patterns are consistent with PC 1 being negatively correlated with the daily change in 700 hPa temperature ($R = -0.62$, Table 3) and with the amplitude of fluctuations being largest in the winter, reflecting more pronounced temperature variations during this season of storm activity.

3.2.2. EOF 2: Opposing East Side and West Side Temperature Deviations

[22] The second mode (EOF 2, 7.0% of the variance, Figure 4b) represents differences in surface temperature deviations between the west slope and the east slope of the Sierra. Seasonally, there is a tendency for positive PC 2 (west slope warm, east slope cool) to dominate in winter and the opposite pattern to dominate in summer (Figure 5b). The magnitude of synoptic scale oscillations tends to be largest during the cool season, reflecting more active storm disturbances.

[23] The second mode (EOF 2) is correlated with the wind direction across the Sierra Nevada ($R = -0.46$ with zonal winds, Table 3). In general, east slope stations are warmer than west slope stations at a comparable elevation (Figure 2), due to the primarily westerly wind over the mountain range, which often results in mountain wave

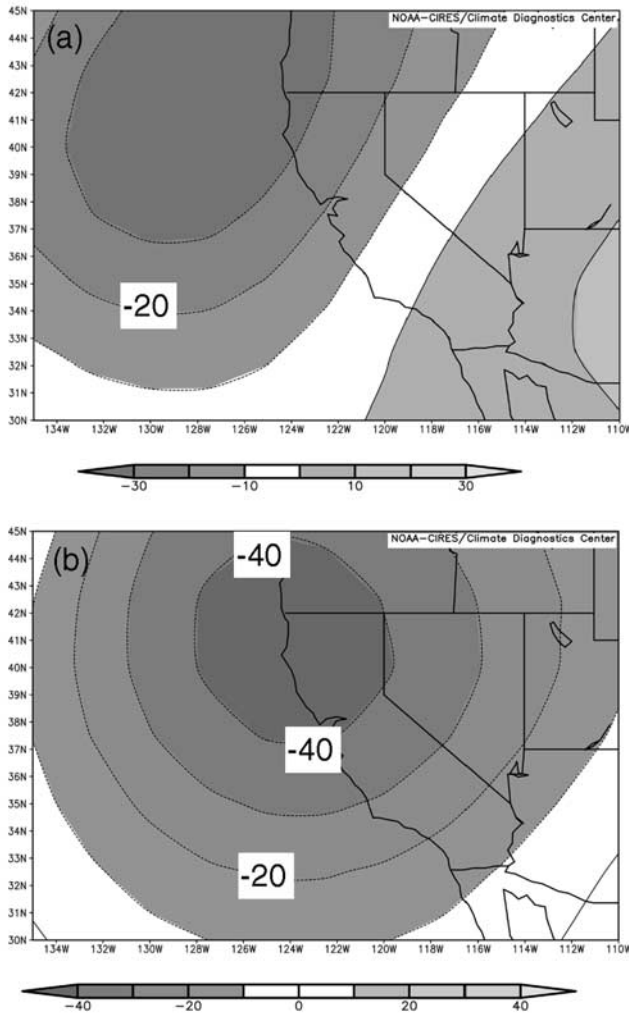


Figure 6. Average 700 hPa height anomalies (m) on (a) the days prior to and (b) the days with PC 1 more than 1 standard deviation above the mean.

development and subsidence over the lee slope, leading to adiabatic warming as the air descends. Positive PC 2 values, when the western sites are relatively warmer and the eastern sites are relatively cooler than average, are associated with a north-easterly tilted ridge replacing a south-westerly tilted trough, resulting in geopotential height contours that form a “backwards-S” pattern over California (Figure 7a) and a large-scale temperature gradient (not shown) with warmer temperatures toward the west. This results in the interruption of the westerly zonal wind flow over the Sierra Nevada (Figure 7b), which stops the more-typical, descending air over the eastern Sierra and instead allows cool air to accumulate against the base of the east slope. Negative PC 2 occurrences, when the western sites are relatively cooler and the eastern sites are relatively warmer than average, correspond to days with strong westerly winds, with geopotential height contours nearly perpendicular to the range (Figure 7c). The illustrated height patterns are the average of many different patterns of 700 hPa troughs and ridges over California, where the unifying feature is that days associated with positive values of PC 2 have easterly winds or very weak westerlies, and days associated with negative values of PC 2 have stronger than average westerly winds. Days with the largest positive values of PC 2 occur when a ridge replaces a trough, as shown in the composite (Figure 7b).

[24] Average temperature anomalies for days with PC 2 values greater than one standard deviation above (Figure 8a) and below (Figure 8b) the mean vary by elevation. In general, higher elevation stations, those closest to the ridgeline, have smaller temperature anomalies than lower-elevation stations on either side of the range, indicating that the west-east contrast is accentuated at downslope and farther separated locations. Negative values of PC 2 occur more often on cold days, but the west slope is much cooler than the east. The occurrence of stronger amplitudes at lower altitudes and during winter may be due to cold air becoming trapped on one side of the Sierra Nevada divide, decoupling the temperatures on the two slopes. This east-versus-west pattern does not emerge in analysis of the daily temperature range, suggesting that east-west contrasts act

Table 3. Correlation Coefficients (*R*) of Normalized 700 hPa Reanalysis Data With PCs^a

Correlations (Whole Year Winter/Summer)	PC 1 (Free-Air Versus Surface)	PC 2 (West-East)	PC 3 (Cold-Air Drainage)	PC 4 (Strengthen-Weaken Lapse Rate)
Temperature (<i>T</i>)	0.08	0.02	0.36	-0.08
Zonal Wind (<i>U</i>)	<u>0.12</u>	-0.46	-0.07	<u>-0.22</u>
Meridional Wind (<i>V</i>)	0.22	0.05	0.19	<u>-0.27</u>
Geopotential Height (Ht)	-0.19	0.12	0.33	-0.03
Relative Humidity (RH)	0.19	0.05	-0.28	-0.04
Specific Humidity (SH)	0.27	0.13	0.05	-0.02
Omega Vertical Velocity (Positive = Sinking Air)	-0.26	-0.06	-0.12	0.22
Lag <i>T</i>	0.31	0.09	0.44	-0.19
Lag <i>U</i>	0.06	<u>-0.54</u>	-0.22	<u>-0.09</u>
Lag <i>V</i>	0.47	-0.06	<u>0.09</u>	<u>-0.29</u>
Lag Ht	0.03	0.21	<u>0.49</u>	-0.19
Lag RH	0.06	-0.07	-0.51	0.01
Lag SH	0.32	0.07	-0.08	-0.07
Lag Omega	-0.51	0.10	0.05	0.25
<i>T</i> change	-0.62	-0.20	-0.23	0.30

^aLags represent correlation with value on prior day. Underlined values are significant at $p < 0.05$, and bold values are significant at $p < 0.01$.

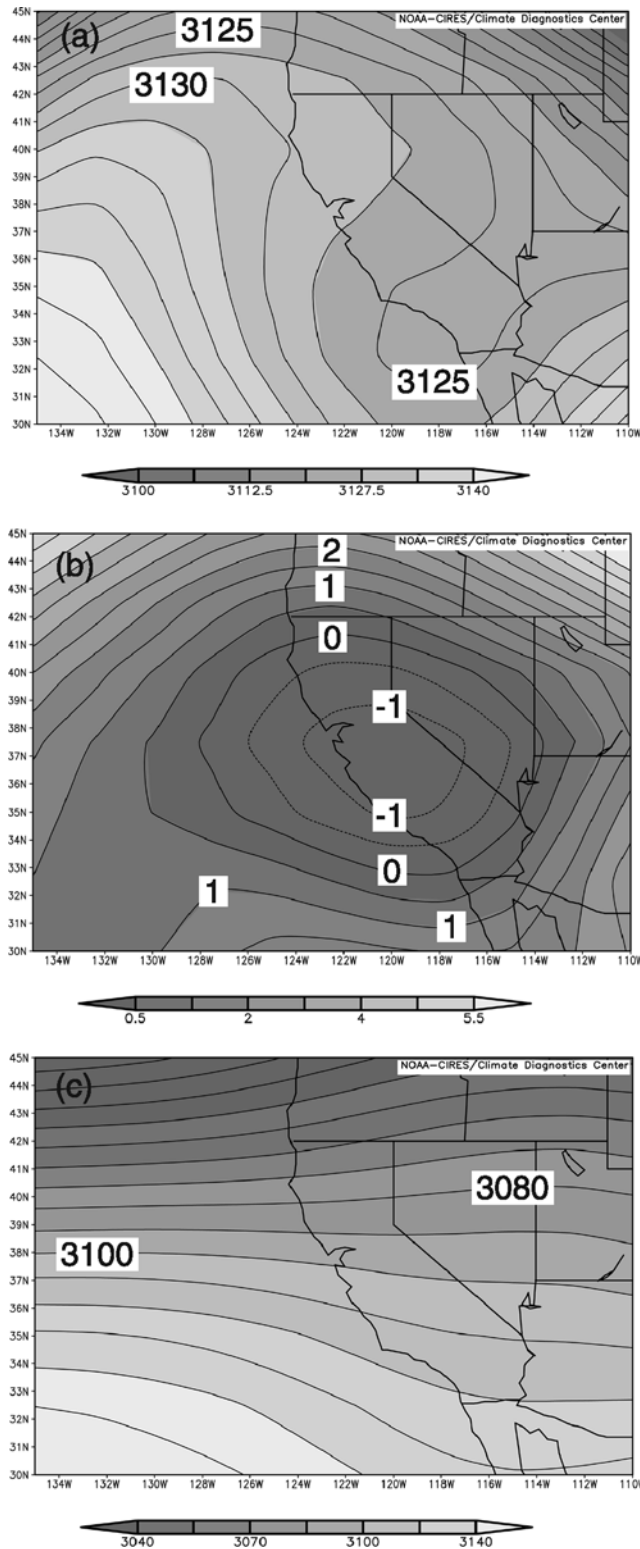


Figure 7. (a) Mean 700 hPa geopotential heights (m) on days with values of PC 2 more than 1 standard deviation above the mean. (b) Mean 700 hPa zonal winds (m s^{-1}) on the same days as in Figure 7a. (c) Mean 700 hPa geopotential heights (m) on days with values of PC 2 < 1 standard deviation below average.

evenly over the entire 24-hours and are not stronger during day or night.

3.2.3. EOF 3: Cold-Air Drainage

[25] The third mode (EOF 3, 3.3% of the variance, Figure 4c) identifies areas that are well-drained, in contrast to those that are prone to accumulation of cold-air, such as the Tuolumne Meadows region of Yosemite National Park (Figure 1, large circles in Figure 4c). These are the areas that were exceptionally cold during the 4–6 January 2004 case study. Occurrences of positive PC 3 were strongest when positive geopotential height anomalies, i.e., anomalously high pressure and anomalously low humidity air masses, were seated over the western USA the previous day, evidenced by correlations with prior day 700 hPa geopotential height ($R = 0.49$, Table 3) and with the prior day relative humidity ($R = -0.51$, Table 3). This is consistent with prior results, which have shown that cold-air drainage occurs most prominently in dry-air, clear-sky conditions with weak synoptic activity [Barr and Orgill, 1989; Anquetin *et al.*, 1998] and is more pronounced downslope of converging canyons, which feed cold air into a downslope valley [Neff and King, 1989], such as the flat, wide, U-shaped valley of Tuolumne Meadows. Fluctuations associated with PC 3 tend to be more frequent and pronounced during the winter months (Figure 5c). Strong negative anomalies are likely related to winter storms (low geopotential heights and humid air masses), and strong positive anomalies may occur because basins with winter inversions are often capped by low clouds, which decrease solar insolation and allow the inversions to strengthen [Whiteman *et al.*, 1999; Neff and King, 1989].

[26] The average hourly temperatures on days with PC 3 values greater than one standard deviation above the mean (Figure 9a, $N = 107$) and less than one standard deviation below the mean (Figure 9b, $N = 127$), for representative stations in Tuolumne Meadows (Budd Creek, 2600 m) and along the west (T14 Ridge, 2400 m) and east slopes (Power Plant Road, 2250 m), clearly correspond to changes in nocturnal drainage, which disproportionately cool the meadow locations. Thus, on days with positive values of PC 3, the diurnal range of temperature is much larger at all stations, and particularly at meadow locations. Composites of multiple stations from each area yield the same results. The diurnal structure of EOF 3 results in stronger variance in minimum temperatures (5% of the variance explained) and temperature range (3.6% of the variance explained), but the EOF 3 pattern does not emerge in an analysis of maximum temperatures.

3.2.4. EOF 4: Strengthening-Weakening of Lapse Rate

[27] The fourth mode (EOF 4, 2.9% of the variance, Figure 4d) correlates well with elevation. Positive values represent a strengthening, and negative values represent a weakening of the temperature lapse rate. PC 4 has the largest amplitude oscillations in the winter months (Figure 5d) and is weakly correlated with the prior-day meridional wind ($R = -0.29$, Table 3) and the current-day vertical velocity ($R = 0.22$, where positive values indicate sinking air, Table 3). Thus positive/negative values of PC 2 have a weak association with northerly/southerly winds and sinking/rising motions. This is consistent with work in the Rocky Mountains by Pepin and Losleben [2002], who found that

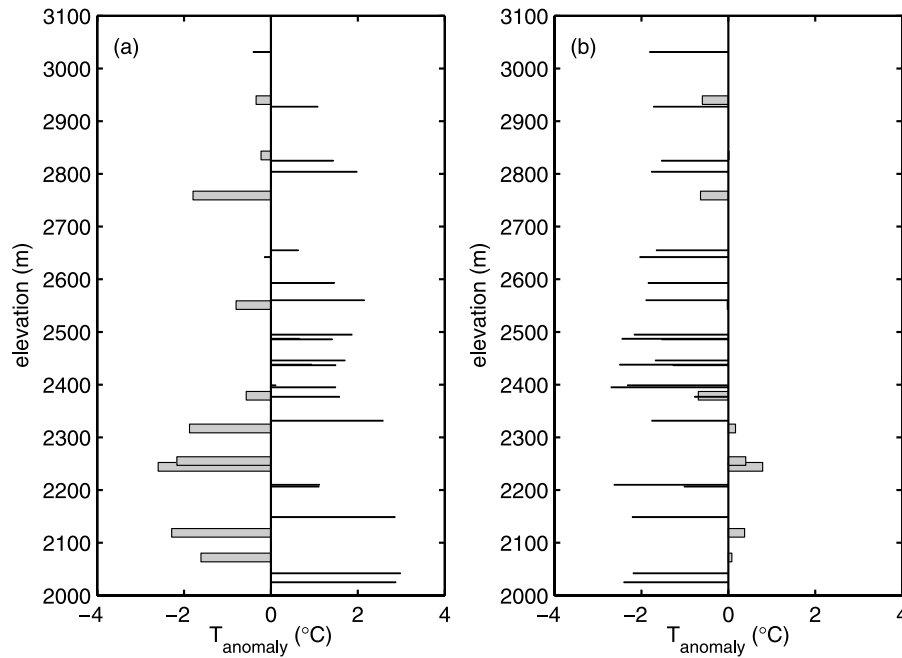


Figure 8. Average temperature anomalies ($^{\circ}\text{C}$) on days with (a) values of PC 2 greater than 1 standard deviation above the mean and (b) days with PC 2 values less than 1 standard deviation below the mean. Grey boxes represent east slope stations; black lines represent west slope stations.

synoptic events with northerly winds, associated with polar air masses, had steeper lapse rates.

3.3. Downscaling and Validation

[28] Because most mountain regions lack a high density temperature network, it is of interest to determine if the spatial temperature structure can be defined by larger scale atmospheric circulation measures, represented here by Reanalysis 700 hPa variables. The variables selected by stepwise linear regression (section 2.3) were generally consistent with the patterns and mechanisms identified in the diagnostics of the EOFs and their PCs in section 3.2 (Table 4). These regression models were able to explain 60, 55, 36, and 14% of the variance of EOFs 1, 2, 3, and 4, respectively, for the July 2002–June 2004 training period. Using multiple linear regression with all terms retained or using nonlinear regression with quadratic combinations of the forcing terms did not increase the explained variance. Because only the first two EOFs could be forecast with over 50% of the variance explained, the discussion in the subsequent sections is limited to these first two EOFs.

[29] Model skill was determined by calculating RMSEs for the representative west, east, and meadow stations for both the 2002–2004 test period and the 2004–2005 validation period. Base state temperatures (estimated using station mean temperatures modulated by 700 hPa Reanalysis temperature variations), had 2002–2004 RMSEs ranging from 1.77°C at the west slope stations to 3.12°C at the east slope stations (Table 5). Adding temperature perturbations represented by EOF 1 reduced the RMSEs to 1.13°C (west slope) and 1.33°C (east slope) when using the original calculated PC 1 values and to 1.37°C (west slope) and 2.23°C (east slope) when PC 1 is modeled using regression equations. Adding perturbations represented by both EOF 1

and EOF 2 reduced the error to $0.80/1.16^{\circ}\text{C}$ at west slope stations and to $0.74/2.16^{\circ}\text{C}$ at east slope stations, where the first value indicates the RMSE if the PCs are known perfectly and the second value if the PCs are modeled.

[30] EOFs 1 and 2 contributed larger incremental improvements to the estimated temperature patterns on days that were poorly represented by the standard lapse rate. During the 2002–2004 test period, 99 days had a RMSE (based on observed temperatures versus those predicted by the standard lapse rate) greater than 2.94°C , which is one standard deviation above the mean. The mean RMSE for these 99 days averaged over all stations was 3.25°C , varying from 2.06°C at the west slope stations to 4.70°C at the east slope stations. On these days, RMSEs for temperatures calculated from the base state and EOF 1 were $1.48/1.52^{\circ}\text{C}$ for west slope stations and $1.81/3.41^{\circ}\text{C}$ for east slope stations. The addition of EOF 2 reduced these errors to $0.98/1.26^{\circ}\text{C}$ (west slope) and $0.96/3.06^{\circ}\text{C}$ (east slope), which were incremental reductions of $0.50/0.26^{\circ}\text{C}$ and $0.80/0.35^{\circ}\text{C}$, about 0.20°C greater error reductions than the average reductions for all cases. Thus the EOF analysis helped more at the times when it was needed most.

[31] The 2004–2005 testing period had larger errors than the 2002–2004 developmental period, perhaps because 2004–2005 was a cooler, wetter year with different storm patterns that were not well represented by the model relationships. RMSEs in the base model ranged from 1.79°C for the west slope stations to 3.49°C for the east slope stations. The first two modeled PCs reduced these errors by increments similar to the error reductions from the modeled PCs obtained during the calibration period. PC 1 reduced the error to 1.52°C (west slope) and to 2.58°C (east slope). The addition of PC 2 further reduced the error to 1.29°C (west slope) and to 2.50°C (east slope), which were

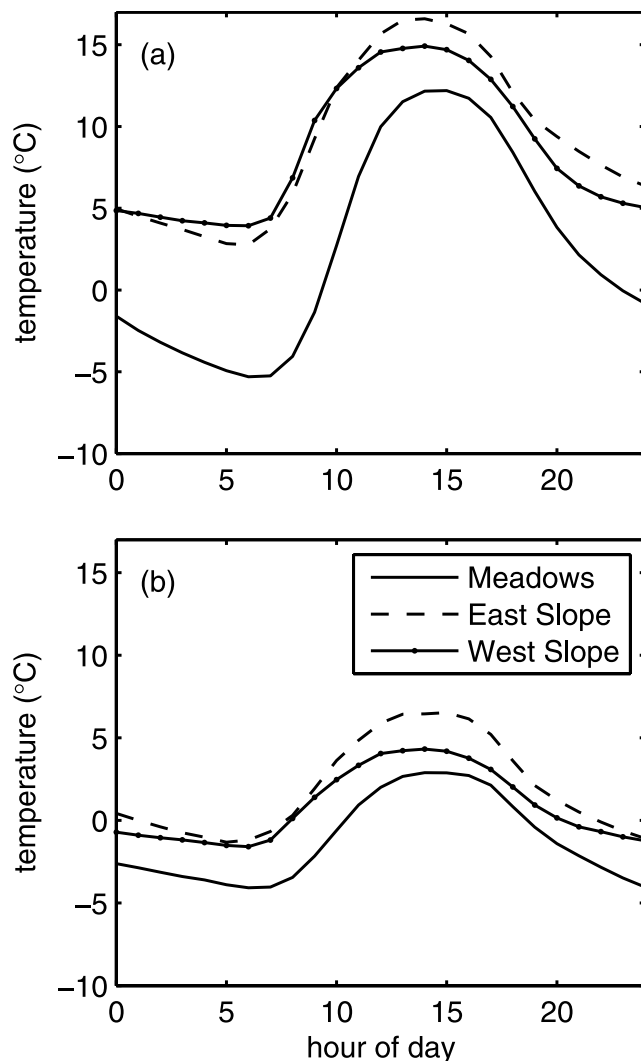


Figure 9. Average hourly temperatures ($^{\circ}\text{C}$) in PST at representative stations on days with (a) PC 3 values > 1 standard deviation above average and (b) PC 3 values < 1 standard deviation below average. Notice the much greater differences in minimum temperatures and diurnal range between the three different regions during days with high PC 3.

incremental reductions of 0.23°C on the west slope and 0.08°C on the east slope. As before, error reductions were greater for days that were very poorly predicted by a standard lapse rate. These analyses indicate that the first two PCs estimated using regression equations based on 700 hPa Reanalysis data can improve the description of temperatures across the Yosemite network during times with limited surface data.

3.4. Hindcasting: Interannual-Decadal Variability Across the Landscape

[32] The prior sections demonstrated that the first two patterns of spatial temperature variability are reasonably well-correlated with large-scale weather patterns and can be estimated using a simple linear model employing 700 hPa Reanalysis variables. Specifically, analysis of EOF 2 demonstrated that changes in westerly winds over the Sierra affect temperatures on the east and west slopes of the mountain range differently. Thus long-term trends in large-scale circulation patterns, specifically trends in the wind direction and strength, will affect temperature trends differently at different mountain locations.

[33] To consider possible variability in Yosemite region temperatures over a much longer period than the limited duration of higher density in situ observations, temperature deviations were estimated for the last six decades (1948–2005) using historical Reanalysis parameters and the regression equations presented above. The estimated PC time series for EOFs 1 and 2 both contain strong interannual and decadal variability (Figure 10). Thus temperature records from a subset of these six decades could exhibit different apparent trends at different locations due solely to changes in large-scale weather patterns.

[34] For example, the reconstructed version of PC 2 exhibits an increasing trend from the mid-1970s until present, particularly during the past 10 years, due to weakening westerly winds, suggesting that temperatures on the east and west slopes of the Sierra have undergone contrasting tendencies during this period. To illustrate, consider the last 10 years (1996–2005) of modeled PC 2 (Figure 10b), when the magnitude increased from -0.2 to 0.05 . Now consider three stations at different locations in Yosemite (Figure 1). Aspen Grove, at 2200-m elevation on

Table 4. Regression Coefficients for Predicting Temporal PCs (0 Represents not Used in Stepwise Regression)

Coefficients (Whole Year)	PC 1 (Free-Air Versus Surface)	PC 2 (West-East)	PC 3 (Cold-Air Drainage)	PC 4 (Strengthen-Weaken Lapse Rate)
Temperature (T)	0	-0.451	0	0
Zonal Wind (U)	0	-0.285	0	0
Meridional Wind (V)	0	0	0	-0.113
Geopotential Height (Ht)	0	0.437	0	0
Relative Humidity (RH)	0	0	0	0
Specific Humidity (SH)	0	0	0	0
Omega Vertical Velocity (Positive = Sinking Air)	0	-0.166	0	0
Lag T	-1.992	0	0	0
Lag U	0	-0.325	0	0
Lag V	-0.359	-0.141	0	0
Lag Ht	1.897	0.000	0.168	0
Lag RH	0	0.159	-0.182	0
Lag SH	-0.501	0	0	0
Lag Omega	0	0	0	0
T change	1.180	-0.387	-0.106	0.136
R^2 (Variance Explained)	60%	55%	36%	14%

Table 5. Root Mean Squared Errors (RMSE) Calculated for Five-Station Groups From the West Slope, East Slope, and Meadows Regions^a

	West (Calculated PCs)	West (Estimated PCs)	East (Calculated PCs)	East (Estimated PCs)	Meadow (Calculated PCs)	Meadow (Estimated PCs)
<i>2002–2004 Calibration Period</i>						
Base State	1.77	1.77	3.12	3.12	2.45	2.45
EOF 1	1.13	1.37	1.33	2.23	0.92	1.76
EOF 2	0.80	1.16	0.74	2.16	0.87	1.73
EOF1–EOF2 Improvement	0.33	0.21	0.60	0.07	0.04	0.03
<i>2004–2005 Validation Period</i>						
Base State		1.79		3.49		2.55
EOF 1		1.52		2.58		1.83
EOF 2		1.29		2.50		1.79
EOF1–EOF2 Improvement		0.23		0.08		0.04

^aAll values are in degrees Celsius. Rows marked “EOF 1–EOF 2 Improvement” demonstrate the reduction in RMSE resulting from adding in EOF 2 to the temperature predicting equation.

the eastern side of the Sierra near Lee Vining, responds to EOF 2 with a factor of -2.1 , so that an increase in PC 2 would result in a decrease in temperature at Aspen grove. Crane Flat, at 2000-m elevation on the western side of the Sierra, responds to EOF 2 with a factor of 1.5 , so an increase in PC 2 would result in an increase in temperature at Crane Flat. Tioga Pass, at an elevation of 3000 m along the Sierra Crest, responds to EOF 2 with a factor of -0.1 , so any change in PC 2 would have very little effect on Tioga Pass temperatures. Over this 10-year period, due mainly to decreasing westerly winds, temperatures at Aspen Grove would be expected to decrease 0.6°C relative to the free air, while temperatures at Crane Flat would be expected to increase 0.4°C relative to the free air, resulting in a 1°C greater difference between the stations. Temperatures at Tioga Pass would not be affected. Thus assuming that overall, the region warmed during this period, anomalous zonal winds (i.e., PC 2) would make it appear from observations along the west slope of the Sierra that higher elevations (for example, Tioga Pass) were warming less rapidly than lower elevations (for example, Crane Flat) over the past 10 years. On the other hand, from observations along the east slope of the Sierra, one would conclude that higher elevations (for example, Tioga Pass) were warming more rapidly than lower elevations (for example, Aspen Grove). This example illustrates the difficulty in interpreting climatic trends with limited stations in complex terrain.

[35] To test how well these long-term modeled spatial differences match observations, monthly average temperatures were obtained from the Hetch Hetchy and Cherry Vale Dam cooperative observing stations on the west slope and from the Mono Lake (prior to 1988), Lee Vining (new location for Mono Lake site, post-1988), and Bodie cooperative observing stations on the east slope. The resulting index time series covered 1955 to 2005. After removing the mean from each time series, the two west-side stations and two east-side stations were averaged (using only one record when the second was missing) to create continuous records for each side of the mountain range. For the 2002 to 2005 period, these records were compared with monthly averages from the five-station east and west composites used in the error analyses above. The east-side composites were correlated at $R^2 > 0.99$, and the west-side composites were correlated at $R^2 > 0.98$. The difference between the east

and west slopes for the coop composites and the five-station composites were correlated at $R^2 = 0.55$, with $p < 0.01$. For the 2002–2005 period, the differences between the five-station-network composites were about twice as large as the differences between the two-station coop composites,

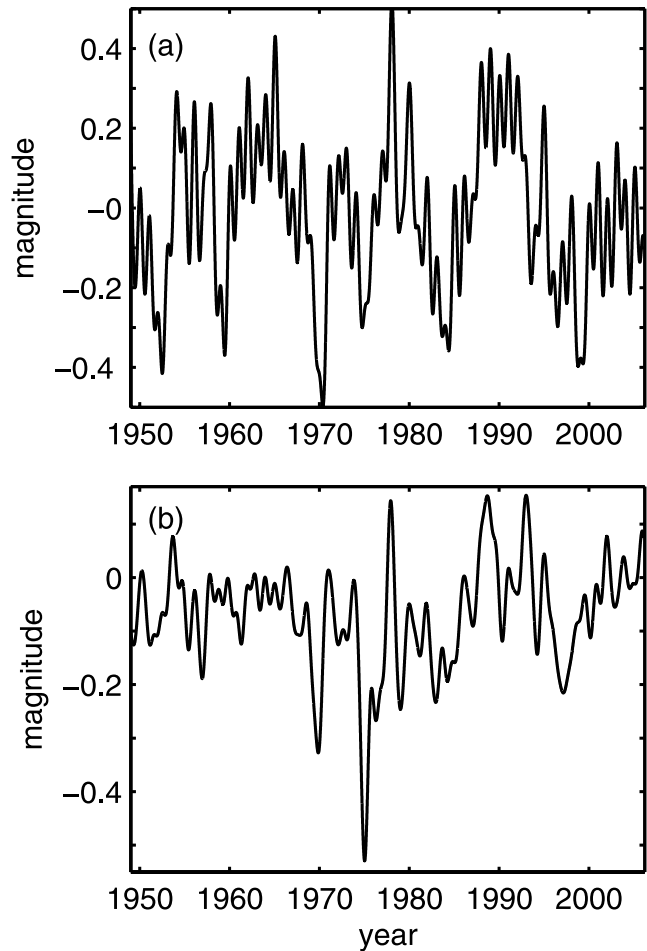


Figure 10. Regression-based PCs of (a) EOF 1 and (b) EOF 2 calculated from Reanalysis data from 1949 to 2005. The data have passed through a low-pass filter with a 2-year Blackman window.

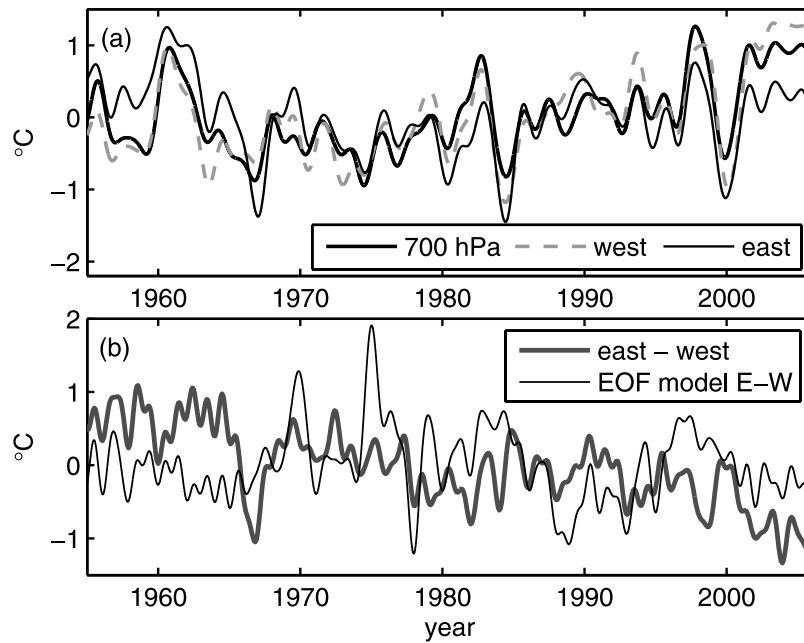


Figure 11. (a) Temperature anomalies from 700-hPa Reanalysis temperatures, east-slope composite cooperative monthly temperatures [Bodie-Lee Vining-Mono Lake], and west-slope composite cooperative monthly temperatures [Hetch Hetchy-Cherry Creek Dam]. (b) Difference between observed east and west composite temperature anomalies and difference between modeled (based on EOFs and Reanalysis) east and west temperature anomalies, which are weakly correlated at $R = 0.17$. Data were filtered as in Figure 10, except the Blackman window in Figure 11 was increased to 3 years to remove the annual temperature cycle.

suggesting that actual long-term differences between the slopes could be larger than the differences portrayed by the existing data.

[36] After removing the long-term mean from all of the time series, the coop composite monthly temperature series were low-pass filtered and compared with filtered 700 hPa temperatures (Figure 11a). All three temperature series have been trending upwards since the mid-1970s. However, the relative sizes of the east slope versus the west slope temperature anomalies have reversed, from the east slope having as much as a 1°C warmer anomaly than the west slope early in the record to the east slope having about a 1°C cooler temperature anomaly late in the record. The Reanalysis temperatures more closely track the west-side observations, perhaps because the closest radiosonde station, Oakland, is located west of the Sierra, or perhaps because the east slope is more decoupled from the free atmosphere. Thus it appears that the regional warming trend over the past 30 years, indicated in Figure 11a, has been subdued on the east slope of the Sierra, and accentuated on the west slope. Temperature differences estimated from the regression model for this period, while also showing a decreasing trend, only correlate with observed differences at $R = 0.17$ ($p < 0.001$, but nonetheless a very weak correlation, Figure 11b). The Reanalysis zonal winds (not shown) are better correlated with the observed temperature contrast, with $R = 0.33$ at $p < 0.001$. While there is still a tendency for anomalous easterly winds to preferentially reduce temperatures on the east slope, the regression model developed from daily Reanalysis variables may not apply very well to

longer timescales, such as monthly or yearly averages, particularly during periods when conditions deviated from those observed in recent years.

3.5. Potential Sources of Analysis Error: Spatial Sampling, Sensor Types, and Microclimate

[37] The temperature sensors in the Yosemite network are concentrated along road and river corridors and are not distributed evenly across the landscape. We tested the robustness of the EOF-analysis by subsampling the number of stations (randomly selecting just 20, just 14, and then only 6 stations) and rerunning the analysis. In any subset containing stations on both slopes, the first two EOFs remained the same. The third and fourth EOFs were not consistent among sample sets containing less than 20 stations. When the analysis was limited to east slope stations, the second EOF highlighted differences between coop stations and other types of stations (3.7% of the variance), for reasons discussed further below. When the analysis was limited to west slope stations, the second EOF (5.8% of the variance) highlighted differences between most stations and the Tuolumne Meadows region (cold-air drainage identified previously in EOF 3). This pattern emerged in any subsample of west slope sites that included at least one Tuolumne Meadows station. The third EOF on the west slope (3.4% of the variance) identified differences between the coop stations and other station types.

[38] Differences between the coop records and that of other sites may be due to sampling frequencies or to microclimate effects. Coop observers typically record the

maximum and minimum temperatures once a day (around 0 UTC) and then reset the thermometers. Sometimes the calendar day maximum or minimum occurs between that time and local midnight, which would result in it being associated with the following day [Karl *et al.*, 1986]. While the coop temperatures were based solely on the average of the maximum and minimum, the daily averages at the automated sensors consisted of 24 or 48 measurements falling within the local calendar day. Coop station thermometers also tend to be lower to the ground and closer to populated areas than the temperature sensors at other locations in the network.

[39] In addition to variations in sampling frequencies, this temperature set encompassed varied environments, with some sensors in meadows/clearings and some in forests/trees, with different albedos, different wind protection, different shelters from solar radiation, and a range of heights above ground level. Sensors were distributed between lower montane (~1000–2100 m, Ponderosa Pine), upper montane (~2100–2600 m, Red Fir, Jeffrey Pine, Western Juniper), and subalpine (~2600–3000 m, Lodgepole Pine, Whitebark Pine, Mountain Hemlock) forests on the west slope, and between upper montane (~3000–2600 m), lower montane (~2600–2100 m), and piñon pine, juniper, and aspen (<2100 m) forests on the east slope (elevation zones marked in Figure 1). While these instrumental conditions and variations in vegetation cover had less effect on the recorded temperatures than the setting of stations on the landscape, i.e., EOF modes highlighting differences between types of sensors accounted for much smaller fractions of the variability than the landscape-scale modes presented here, sensor differences could be a potential source of error. To check for such error, the EOF analyses were recalculated for subsets of stations consisting of just one type of sensor (for example, just snow pillow stations, or just tidbit sensors). Each subset, provided that it spanned the controlling landscape characteristics (east and west slopes, at least one station in Tuolumne Meadows, and a range of elevations), possessed the same modes of spatial variability presented above (EOFs 1 to 4). One possible explanation for the insignificance of vegetation-controlled microclimate in this data set could be because all of the sensors were at the edges of vegetation patches (for example, along a road or river corridor), where temperatures are less modified than those in interior forest locations [Chen *et al.*, 1999].

4. Summary of Major Results and Their Significance

[40] A prototypical network of temperature sensors distributed across the Yosemite National Park region of the central Sierra Nevada, California revealed spatial and temporal variations of the surface temperature residuals from temperatures in the free atmosphere at the 700 hPa level. Although the study was based upon a short (2002–2005) record, some general conclusions can be drawn. While on average, temperatures across this complex terrain vary according to the standard linear lapse rate; this is often not an adequate prescription of temperature on a given day. As an alternative to the standard lapse rate representation, four spatial patterns of the temperature residuals were isolated using empirical orthogonal function (EOF) analy-

sis. Each of the patterns identified was correlated with particular variables relating to the larger-scale atmospheric circulation. The four patterns include (1) a strongly predominant pattern of residual temperature variability in which the surface over the entire region is cooler or warmer than the free atmosphere, (2) the west slope is anomalously warmer or cooler than the east slope, (3) preferential cooling in locations where cool nocturnal air can drain into and pool, and (4) an exaggerating or muting of the average vertical temperature lapse rate. While the latter two patterns account for small fractions of the total variance, they, like the first two EOFs, appear to have physical bases that are likely to be applicable in many mountain ranges. The third pattern represents some extreme events, such as the 4 January 2004 event (Figure 3). The observations demonstrate that cold-air drainage can reduce the surface temperature, relative to the free atmosphere, in flat meadows and valleys by up to 15°C during cool, calm high-pressure events.

[41] Multiple linear regression models were used to relate the PCs of each of the first two EOFs to 700 hPa Reanalysis variables in order to downscale the broader scale atmospheric circulation to spatial temperature patterns across the landscape. Although there may also be finer scale circulations that play a role in determining the surface temperature variability, these models indicate that some easily obtained measures from the large scale circulation provide additional skill relative to standard techniques. RMSEs of temperatures predicted with modeled EOFs 1 and 2 were on average 0.84°C/0.43°C smaller on the west/east slopes than temperatures predicted by the standard lapse rate, and 0.61°C/0.96°C smaller than temperatures estimated from Reanalysis data adjusted by each station's 2-year mean temperature, referred to here as the "base state." While these methods provide relatively small improvements on average, they provide larger incremental improvements on days that are poorly represented by a linear lapse rate.

[42] As gauged by the variability recorded by the Yosemite network, decadal-scale changes in atmospheric circulation patterns appear to have affected the temperature contrast across the east and west sides of the Sierra Nevada range. This change may have contributed to a trend toward less long-term warming on the east slope than the west slope of the Sierra Nevada. This may help to explain why spring melt timing has advanced more rapidly on the west slope than on the east slope of the Sierra Nevada [Stewart *et al.*, 2005; Stewart, personal communication, 2006].

[43] The complex temperature structure exhibited by the Yosemite network indicates the need for much higher density observations in mountainous terrain than is presently available in most locations. Fortunately, temperature is relatively easy and inexpensive to monitor. The results here indicate that only a few years of higher density data yield a useful portrait of the temperature variability that cannot be obtained from the sparser array of stations that is typical of mountain settings. The techniques presented could be applied to other mountainous regions, including higher elevations, where spatial patterns may help determine why neighboring glaciers are retreating at different rates. It is left to be demonstrated, but the results of this study suggest that spatial surface temperature patterns from a representative sampling array, combined with larger scale atmospheric

circulation measures, can be used to identify key topographically controlled temperature patterns, and thus to estimate temperatures at arbitrary points on the landscape. Moreover, because key aspects of the spatial surface temperature structure are governed by large-scale circulation, it may be possible to use routine weather data to estimate surface temperatures at times when the distributed sensor information is not available.

[44] The methods presented here may also be useful in studies of forest ecosystems and landscape ecology, which grapple with variations in microclimate across many spatial and temporal scales [Chen *et al.*, 1999]. Because low-cost sensor networks provide a better estimate of regional variations in temperature through space and time, similar networks should be useful for understanding spatial distributions of biota across the landscape. They could also be used to determine the primary modes of temperature variability on different scales (i.e., different subsets of the sensors), which could then be incorporated into landscape models.

[45] A higher density network of mountain surface temperatures has many applications, including: (1) filling gaps in temperature records when a station has malfunctioned, (2) providing input to spatially distributed snowmelt models, many of which are based on temperature (such as the Snow-17 model used in operational forecasting [Anderson, 1976]), (3) improving spatial downscaling techniques for climate models, which currently rely upon fixed lapse rates, (4) informing studies of vegetation and ecosystems, which respond to small-scale changes in temperature, and (5) potentially, interpreting long-term temperature trends at various locations across the mountain landscape.

[46] **Acknowledgments.** Thank you to Andrey Shcherbina for help programming the EOF calculations. Thank you to Connie Millar, Bob Westfall, Randy Dole, Nick Pepin, and two anonymous reviewers for editorial comments and suggestions. NCEP-NCAR Reanalysis data were provided by the NOAA-CIRES ESRL/PSD Climate Diagnostics branch, Boulder, Colorado, USA, from their Web site at <http://www.cdc.noaa.gov/>. California Cooperative Snow Surveys data were provided by Frank Gehrke of the California Department of Water Resources: RAWS data were provided by Kelly Redmond from the Western Regional Climate Center. Jenn Kelley helped download data sets. Thank you to Brian Huggett, Heidi Roop, Frank Gehrke, Jim Roche, Larry Riddle, Jim Wells, Mike Dettinger, Alex Revchuk, and Julia Dettinger for field work and temperature sensor installations. Funding was provided to JDL by a Canon National Parks Science Scholarship, a CIRES postdoctoral fellowship, the Edna Baily Sussman Foundation, and by Cal-IT2. Funding for DRC was from the NOAA Climate Program Office, the NSF RoadNET program, and the California Energy Commission PIER Program.

References

Anderson, E. A. (1976), A point energy and mass balance model of a snow cover, Silver Spring, MD. U. S. National Oceanographic and Atmospheric Administration (NOAA) Technical Report NWS 19.

Anderson, E., Z. Bai, C. Bischof, S. Blackford, J. Demmel, J. Dongarra, J. Du Croz, A. Greenbaum, S. Hammarling, A. McKenney, and D. Sorensen (1999), *LAPACK User's Guide* (http://www.netlib.org/lapack/lug/lapack_lug.html), 3rd ed, SIAM, Philadelphia.

Anquetin, S., C. Guilbaud, and J. Cholle (1998), The formation and destruction of inversion layers within a deep valley, *J. Appl. Meteorol.*, *37*, 1547–1560.

Archer, D. (2004), Hydrological implications of spatial and altitudinal variation in temperature in the upper Indus basin, *Nord. Hydrol.*, *35*, 209–222.

Barr, S., and M. M. Orgill (1989), Influence of external meteorology on nocturnal valley drainage winds, *J. Appl. Meteorol.*, *28*, 497–517.

Beckers, J. M., and M. Rixen (2003), EOF calculations and data filling for incomplete oceanographic datasets, *J. Atmos. Ocean. Technol.*, *20*, 1839–1856.

Beniston, M., H. F. Diaz, and R. S. Bradley (1997), Climatic change at high elevation sites: An overview, *Clim. Change*, *36*, 233.

Chen, J., S. C. Sauners, T. R. Crow, R. J. Naiman, K. D. Brosofske, G. D. Mroz, B. L. Brookshire, and J. F. Franklin (1999), Microclimate in forest ecosystem and landscape ecology, *BioScience*, *49*, 288–297.

Daly, S. F., R. E. Davis, E. Ochs, and T. Pangburn (2000), An approach to spatially distributed snow modeling of the Sacramento and San Joaquin basins, California, *Hydrol. Processes*, *14*, 3257–3271.

Daly, C., W. P. Gibson, G. H. Taylor, G. L. Johnson, and P. Pasteris (2002), A knowledge-based approach to the statistical mapping of climate, *Clim. Res.*, *22*, 99–113.

Dettinger, M. D., D. R. Cayan, M. K. Meyer, and A. E. Jeton (2004), Simulated hydrologic responses to climate variations and change in the Merced, Carson, and American River Basins, Sierra Nevada, California, 1900–2099, *Clim. Change*, *62*, 283–317.

Diaz, H. F., and R. S. Bradley (1997), Temperature variations during the last century at high elevation sites, *Clim. Change*, *36*, 253–279.

Draper, N., and H. Smith (1981), *Applied Regression Analysis*, 2nd ed., pp. 307–312, John Wiley, Hoboken, N. J.

Hamlet, A. F., P. W. Mote, M. P. Clark, and D. P. Lettenmaier (2005), Effects of temperature and precipitation variability on snowpack trends in the western U. S., *J. Clim.*, *18*, 4545–4561.

Kalnay, E. (1996), The NCEP/NCAR 40-year reanalysis project, *Bull. Am. Meteorol. Soc.*, *77*, 437–471.

Karl, T. R., C. N. Williams Jr., P. J. Young, and W. M. Wendland (1986), A model to estimate the time of observation bias associated with monthly mean maximum, minimum and mean temperatures for the United States, *J. Appl. Meteorol.*, *25*, 145–160.

Knowles, N., M. D. Dettinger, and D. R. Cayan (2006), Trends in snowfall versus rainfall in the Western United States, *J. Clim.*, *19*, 4545–4559.

Lundquist, J. D., D. R. Cayan, and M. D. Dettinger (2003), Meteorology and hydrology in Yosemite National Park: A sensor network application, in *Information Processing in Sensor Networks*, edited by F. Zhao and L. Guibas, IPSN 2003, LNCS 2634, 518–528.

Martinez, J., and A. Rango (1986), Parameter values for snowmelt runoff modeling, *J. Hydrol.*, *84*, 197–219.

Neff, W. D., and C. W. King (1989), The accumulation and pooling of drainage flows in a large basin, *J. Appl. Meteorol.*, *28*, 518–529.

Pepin, N. (2000), Twentieth-century change in the climate record for the Front Range, Colorado, USA, *Arct. Antarct. Alp. Res.*, *32*, 135–146.

Pepin, N., and M. Losleben (2002), Climate change in the Colorado Rocky Mountains: Free air versus surface temperature trends, *Int. J. Climatol.*, *22*, 311–329.

Pepin, N., and J. R. Norris (2005), An examination of the differences between surface and free-air temperature trends at high-elevation sites: Relationships with cloud cover, snow cover, and wind, *J. Geophys. Res.*, *110*, D24112, doi:10.1029/2005JD006150.

Pepin, N., M. Losleben, M. Hartman, and K. Chowanski (2005), A comparison of SNOTEL and GHCN/CRU surface temperatures with free-air temperatures at high elevations in the Western United States: Data compatibility and trends, *J. Clim.*, *18*, 1967–1985.

Preisendorfer, R. W. (1988), *Principal Component Analysis in Meteorology and Oceanography*, Number 17 in *Developments in Atmospheric Science*, Elsevier, New York.

Richner, H., and P. D. Phillips (1984), A comparison of temperatures from mountaintops and the free atmosphere—Their diurnal variation and mean difference, *Mon. Weather Rev.*, *112*, 1328–1340.

Rolland, C. (2003), Spatial and seasonal variations of air temperature lapse rates in alpine regions, *J. Clim.*, *16*, 1032–1046.

Singh, P. (1991), A temperature lapse rate study in Western Himalayas, *Hydrol. J Indian Assoc. Hydrologists*, *14*, 156–163.

Stewart, I. T., D. R. Cayan, and M. D. Dettinger (2005), Changes towards earlier streamflow timing across Western North America, *J. Clim.*, *18*, 1136–1155.

Whiteman, C. D., X. Bian, and S. Zhong (1999), Wintertime evolution of the temperature inversion in the Colorado Plateau Basin, *J. Appl. Meteorol.*, *38*, 1103–1117.

D. R. Cayan, Scripps Institution of Oceanography, La Jolla, CA, USA.
 J. D. Lundquist, Civil and Environmental Engineering, University of Washington, Seattle, WA 98195-2700, USA. (jdlund@u.washington.edu)